

Chaos-based image encryption using vertical-cavity surface-emitting lasers

Animesh Roy^a, A. P. Misra^{a,*}, Santo Banerjee^{b,c}

^aDepartment of Mathematics, Siksha Bhavana, Visva-Bharati University, Santiniketan-731 235, West Bengal, India

^bMalaysia-Italy Centre of Excellence for Mathematical Sciences, Universiti Putra Malaysia, Malaysia

^cInstitute for Mathematical Research, Universiti Putra Malaysia, Selangor, Malaysia

Abstract

We study the encryption and decryption processes of color images using the synchronization of polarization dynamics in a free-running vertical-cavity surface-emitting laser (VCSEL). Here, we consider a bidirectional master-slave configuration or two-way coupling with two VCSELs. The latter are shown to exhibit hyperchaos and synchronization with a high level of similarity between their emission characteristics. The coupled VCSELs are then used as a transmitter and a receiver for the communication of image or data. Furthermore, we propose a modified chaos-based image encryption algorithm using the pixel- and bit-level permutations which provides robust, faster and simpler encryption/decryption compared to many other chaos-based cryptosystems. The performances of the new cryptosystem are analyzed and compared with a recently developed scheme [Opt. Las. Eng. 90 (2017) 238-246]. The security analysis and some statistical investigations show that the proposed cryptosystem is resistant to various types of attacks and is efficient for secure communications in nonlinear optical media.

Keywords: Image encryption, Bit-level permutation, Surface-emitting laser, Chaos, Synchronization

1. Introduction

The advancement of public communication systems, such as satellite, mobile-phone, computer networking, Internet etc., has led to vulnerability in secure communication of e.g., the transmission of confidential data like military data, confidential videos, messages etc. In this way, the theory of cryptography has been developed (For some recent works, see, e.g., Refs.[1–3, 3–7, 10, 11]). On the other hand, the invention of semiconductor laser diodes, e.g., the vertical-cavity surface-emitting lasers (VCSELs) has been gaining its potential applications in laser devices considering their numerous advantages over Light Emitting Diode (LED) and Edge Emitting Laser (EEL), such as low threshold, circular beam profile, and on-wafer testing capability [12, 13]. Given their electro-optical characteristics and ability to modulate at frequencies ($\gtrsim 25$ Gbps), VCSELs are ideal for high-speed communications and precision sensing applications. They are also used for reliable operation at distances ranging from very close proximity links (i.e., centimeters) up to 500 m in data center, enterprise, and campus networks. Furthermore, such VCSELs have been widely used in data communication industry for more than 15 years serving in data infrastructure links including 10, 40 and 100 Gbps Ethernet, 16 Gbps fiber channel, and 10, 14, and soon 25 Gbps lane Infinite Band. VCSELs are also emerging as an enabling technology across a wide range of applications, including touchless sensing, chip-to-chip interconnect, and gesture recognition.

It has been shown that VCSELs can also exhibit nonlinear polarization dynamics and chaos [6]. Such chaos can be obtained in a number of ways, e.g., when the lasers are driven (into chaos) due to optical feedback from an external reflector. Furthermore, optical lasers like VCSELs or semiconductor lasers are used as secured media for transmission of confidential data, videos, messages etc. These lasers are also used for encryption-decryption of color images in the context of chaos based cryptography [7].

It is to be noted that two identical but independent chaotic systems cannot exhibit the same behaviors unless it is coupled or linked in some ways. In the latter, the system's evolution becomes identical, which is known as the chaos synchronization. Such exciting property of a dynamical system led to the development of secure chaos communication systems where the sender hides a message within the chaotic signal that can only be recovered by the receiver at the synchronized state. This approach has been applied in many secure communications, especially in optical chaos communication systems because of the added security and the speed of optical communications [7, 8].

In classical cryptographic schemes (e.g., AES, DES, One time pad), public key cryptography is widely used for secure networking system. However, these schemes have some limitations in fast encryption on large data scales, such as those in color images, videos or audio data etc. These are not only sequences of large data sets, but also each sequence is highly correlated with another. Encryption of these data set with the classical schemes, as above, takes a longer time and thereby makes the system much slower (see, e.g., Ref. [14]). In order to resolve this issue, many authors have proposed chaos based cryptography schemes [1–4, 9] in which a nonlinear dynamical

*Corresponding author.

Email addresses: aroyiitd@gmail.com (Animesh Roy), apmisra@visva-bharati.ac.in, apmisra@gmail.com (A. P. Misra), santoban@gmail.com (Santo Banerjee)

cal system, which exhibits chaos, is considered for encryption and decryption [6, 7]. On the other hand, the data encryption in chaotic medium is known to be much efficient than the traditional method in which it is more easier for hackers to recover the confidential data. Here, we consider a RGB color image which is a large set of data and its color distribution is highly correlated with the data set. So, although the transmission of these kind of data using the traditional encryption scheme is secured but security is much enhanced if we use a non-pattern medium like chaotic medium.

In this work, we consider a quantum spin-flip model (SFM) of VCSELs [6, 15–17], to be given in Sec. 2, which is used for encryption and decryption of a RGB image using a modified chaos based cryptography scheme. It is shown that the coupled VCSELs can exhibit hyperchaos and synchronization with a wide range of values of the parameters. A new hyperchaos-based image encryption algorithm using the pixel- and bit-level permutations, which modifies the previous one [2], is proposed and tested with an RGB image. It is seen that the new cryptosystem is robust, faster, simpler and more secured in comparison with Ref. [2] and other chaos-based cryptosystems [1–5, 9]. A statistical investigation is also carried out to ensure that the proposed encryption scheme is free from any brute force attack.

2. The model of VCSELs and their chaotic properties

We consider the nonlinear dynamics of right- and left-circularly polarized (RCP, LCP) emission arising from the recombination of two distinct carrier populations D_+ and D_- in VCSELs. The latter have a high quantum efficiency and low threshold which can operate on a very high rate optical communication in the range of several GHz. In terms of the slowly varying electromagnetic (EM) fields E_{\pm} (normalized by the equilibrium value E_0) for RCP and LCP emission, we have the following set of equations [6, 16, 17]

$$\frac{dE_{\pm}}{dt} = \kappa(1 + i\alpha)(N \pm n - 1)E_{\pm} - i\gamma_p E_{\mp} - \gamma_a E_{\mp}, \quad (1)$$

$$\frac{dN}{dt} = -\gamma(N - \mu) - \gamma[(N + n)|E_+|^2 + (N - n)|E_-|^2]|E_0|^2, \quad (2)$$

$$\frac{dn}{dt} = -\gamma_s n - \gamma[(N + n)|E_+|^2 - (N - n)|E_-|^2]|E_0|^2, \quad (3)$$

where $N, n = D_{\pm}$ are the normalized carrier populations, κ is the decay rate of the electric field in the cavity, α is the linewidth enhancement factor, and μ is the normalized injection current. Furthermore, γ is the carrier decay rate, γ_s is the spin-flip relaxation rate which models the process allowing the equilibration of the carrier population between the two reservoirs, and γ_p and γ_a are, respectively, the phase and amplitude anisotropies inside the laser cavity.

In order to establish chaos, we numerically solve the system of Eqs. (1)-(3) by a fourth order Runge-Kutta scheme with a time step size $t = 0.01$ and an initial conditions $E_{\pm} = 0.001$, $N = 0.003$, $n = 0.001$. The typical parameter values are considered as

- $1 \leq \kappa \leq 100 \text{ ns}^{-1}$, $2 \leq \kappa_{inj} \leq 10 \text{ ns}^{-1}$, $\alpha = 3$, $2 \leq \Delta \leq 10 \text{ ns}^{-1}$,
- $0 \leq \gamma_p \leq 100 \text{ ns}^{-1}$, $-7 \leq \gamma_a \leq 7 \text{ ns}^{-1}$, $1.45 \leq \gamma \leq 1.5 \text{ ns}^{-1}$, $0 \leq \gamma_s \leq 100 \text{ ns}^{-1}$.

The results are displayed in Fig. 1 after the end of the simulation at $t = 1000$. From Fig. 1, it is seen that both the polarized electric fields E_{\pm} of the master laser exhibit chaos along with the carrier population densities N and n . It is found that the chaotic state of the system can be reached due to the increasing values of the injection current parameter μ . Furthermore, in order to have some confirmation of our results, we have computed the largest Lyapunov exponents as exhibited in Fig. 2 with the same parameter values as for Fig. 1. It is found that of the four exponents, two are always negative (not shown in the figure), and two others may be positive or negative depending on the values of the injection current parameter μ . From Fig. 2, it is evident that the two lyapunov exponents can turn over from negative to positive values as the values of μ increase, leading to chaos (more specifically hyperchaos) for a longer time. This is in consequence with the fact that the chaos in VCSELs is obtained when the lasers are driven due to the optical feedback from an external reflector.

3. Synchronization of master and slave VCSELs

We investigate the synchronization of two nearly coupled VCSELs, namely the master and the slave lasers which exhibit chaos as in Sec. 2. We call the model Eqs. (1)-(3) as the master VCSEL and couple it with another VCSEL model, called the slave VCSEL, which is very similar to the master one except with some coupling terms $\propto \kappa_{inj}$. Thus, the equations for the slave VCSEL model are

$$\begin{aligned} \frac{dE_{s\pm}}{dt} &= \kappa(1 + i\alpha)(N_s \pm n_s - 1)E_{s\pm} - i\gamma_p E_{s\mp} \\ &\quad - \gamma_a E_{s\mp} - \Delta E_{s\pm} + \kappa_{inj} E_{\pm}, \end{aligned} \quad (4)$$

$$\begin{aligned} \frac{dN_s}{dt} &= -\gamma(N_s - \mu) - \gamma[(N_s + n_s)|E_{s+}|^2 \\ &\quad + (N_s - n_s)|E_{s-}|^2]|E_0|^2, \end{aligned} \quad (5)$$

$$\begin{aligned} \frac{dn_s}{dt} &= -\gamma_s n_s - \gamma[(N_s + n_s)|E_{s+}|^2 \\ &\quad - (N_s - n_s)|E_{s-}|^2]|E_0|^2, \end{aligned} \quad (6)$$

where $E_{s\pm}$ are the electric fields, N_s and n_s are the total and difference of carrier population densities of the slave laser, Δ is the detuning pulsation (difference between the frequencies of the master and slave lasers at the threshold of no anisotropy) and κ_{inj} is the coupling coefficient. Similar to Fig. 1, the system of Eqs. (4)-(6) for the slave laser can also be shown to exhibit hyperchaos with the same set of values of the parameters.

The essential prerequisite for the synchronization of the two systems is that the VCSELs operate in a chaotic regime when subject to an optical feedback. In the case of very low optical

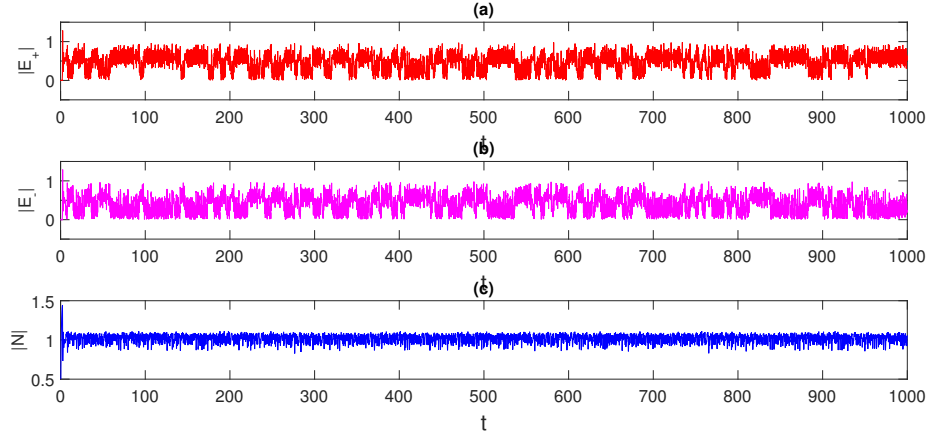


Figure 1: Numerical solution of Eqs. (1)-(3) for the forward and backward electric fields (E_{\pm} , the upper and middle panels) and the carrier population density (N , the lower panel) which exhibit chaos.

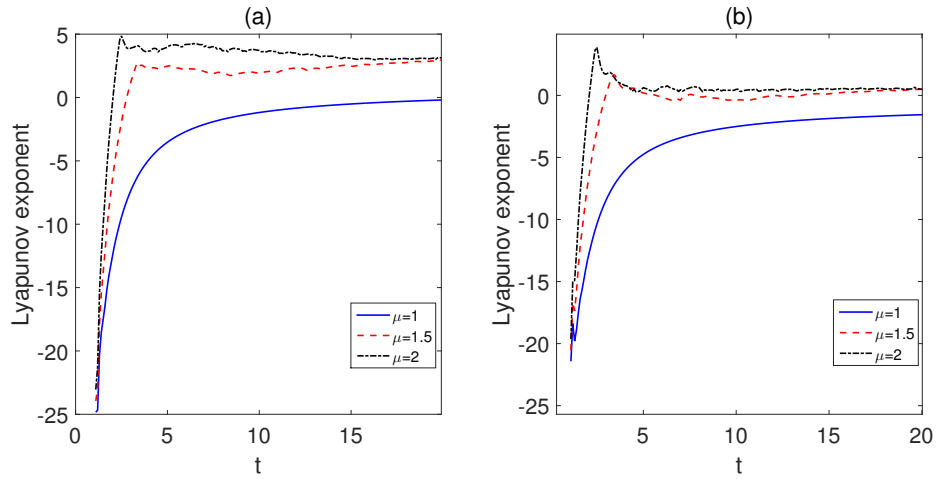


Figure 2: The two Lyapunov exponent spectra, corresponding to the system of Eqs. (1)-(3), are shown with time t in the subplots (a) and (b) for different values of the injection current parameter μ . It is seen that as μ increases, the Lyapunov exponents turn over from negative to positive values. The other two exponents are always negative (not shown) irrespective of the values of μ . The parameter values are taken as $\kappa = 26 \text{ ns}^{-1}$, $\alpha = 3$, $\gamma_s = 5$, $\mu = 1.5$, $\gamma_p = 5 \text{ ns}^{-1}$ and $\gamma_a = -7 \text{ ns}^{-1}$.

coupling, i.e., with a lower values of the coupling coefficient κ_{inj} , the correlation between the outputs of the master and slave lasers is rather poor. However, as the coupling is enhanced with an increased value of κ_{inj} to its optimum value, the correlation is significantly improved and the lasers are said to be synchronized. Further increase in the coupling coefficient may result into “no synchronization”. In the former case, it is apparent that the signal from the master laser is too weak to affect the synchronization, whereas in the latter, the behavior of the slave is too strongly affected by the master laser at the largest value of the coupling coefficient.

Next, we study the synchronization properties of the master and the slave lasers (with suffix s) given by Eqs. (1)-(3) and (4)-(6) which exhibit chaos. These two systems, in fact, describe the driver and response systems for communications in chaotic media through synchronization in VCSELs. In Eq. (4) we have introduced a coupling term with a coefficient κ_{inj} which behaves as a noise-like term. A numerical simulation with an initial condition as for Fig. 1 reveals that synchronization of the two systems is, indeed, achieved after a certain time through the coupling term $\propto \kappa_{inj}$ (See Fig. 3). The parameter values taken are $\Delta = \kappa_{inj} = 10 \text{ ns}^{-1}$. The other parameter values are as for Fig. 1. Basically, Fig. 3 displays the synchronization error between the driving and response lasers at the most chaotic state. It is seen that the corresponding errors for the electric fields and the carrier densities are of the orders of 10^{-15} . Thus, at the state of synchronization the system of Eqs. (1)-(3) can be considered as transmitter and the system of Eqs. (4)-(6) as the receiver one.

4. Transmission of data through chaotic medium

We consider the coupling between two systems of VCSELs for transmission of data. A schematic diagram is given in Fig. 4 to demonstrate how a high resolution data can be transferred from the transmitter (T-VCSEL) to the receiver (R-VCSEL) by means of synchronization of these coupled systems. However, the main concern is that each laser has its own noise which may prevent establishing the synchronization. In order to get rid of this situation, i.e., to reduce the noise from the systems, the optical beam splitter and the optical isolator are used. It has been shown that the VCSEL model has lesser noise emission than the semiconductor lasers [17]. The coupling of the two VCSELs and the transmission of data through chaotic medium are demonstrated step by step as follows:

- Take an RGB image (data) and switch on the transmitter system. The current flows through the laser diode.
- Chaos sequence is formed of the electric fields E_{\pm} and the carrier densities N, n .
- The master laser reads the image pixels as a sequence of data.
- Relate the two sequences of data set, namely the chaotic data and the pixel data with, e.g., an XOR operation. This part is called the encryption.

- Switch on the receiver system (slave laser) and synchronize it with the master laser. Data-pulse then propagates from the master to the slave laser and chaos is established in the slave laser.
- Arrange the chaotic data sequences of the slave laser, and use it to decrypt the image.

In Sec. 5, we will discuss these steps in more detail.

5. Chaos-based image encryption and decryption

In this section we propose an algorithm for encryption of a high quality RGB image. In the latter, we have a three-dimensional matrix $P[m, l, k]$ and all the elements are integer modulo 256, i.e., they lie in between 0 – 255 and are called the voxel values of the image. The color distribution is formed of red (R), green (G) and blue (B). We follow the similar process as in Ref. [2, 7] for the encryption of an RGB image. First, we generate the key vectors by the chaotic system (master laser) and reshape the corresponding matrix as per the size of the image. Then a pixel-level permutation is employed to shuffle the pixel positions of the image. Next, we change the bits of each pixel value of the shuffled sequence by the bit-level permutation matrix in order to strengthen the security of the cryptosystem. Finally, we get the cipher-image by using the BitXOR operation. The encryption and decryption process is shown in Fig. 6. In the following subsections 5.1-5.2 we demonstrate the encryption/decryption scheme in more detail.

5.1. Generation of key for image encryption

We generate the key vectors by the chaotic solutions of the system of Eqs. (1)-(3). When the chaos is established in the master laser, we take all the values of E_{\pm} and N sequentially as vectors to be used in the encryption. Some of these data may be of complex numbers which render the encryption algorithm more difficult to construct. However, we represent the field vectors E_{\pm} and the density vector N in terms of the chaos sequences are as follows:

- $E_{vec}^+ = E_1^+, E_2^+, E_3^+, \dots, E_j^+$.
- $E_{vec}^- = E_1^-, E_2^-, E_3^-, \dots, E_j^-$.
- $N_{vec} = N_1, N_2, N_3, \dots, N_j$, where j is the number of the iteration.
- $K_i^1 \leftarrow (\text{round}(\text{abs}(E_i^+) \times 10^{10})) \bmod(256)$.
- $K_i^2 \leftarrow (\text{round}(\text{abs}(N) \times 10^{10})) \bmod(256)$.
- Generate the key by means of the two sequences of integers K_i^1 and K_i^2 as $K_{yi} \leftarrow (\text{abs}(K_i^1) - \text{floor}(\text{abs}(K_i^2)) \times 10^{10}, \bmod 256)$, where the numbers of elements of K_{yi} vectors are equal to the lengths of the vectors E_+ and N .

It is to be mentioned that in our encryption scheme, we take the image as vectors which are much lower in number than the key vectors. So, we take the key vectors in such a way that all the vectors form a matrix and each column contains at most $m \times l \times k$ vectors, i.e., $K_{y(m \times l \times k)} \leftarrow \text{reshape}(K_y, m \times l \times k, 1)$. This matrix is now used for encryption of the color image.

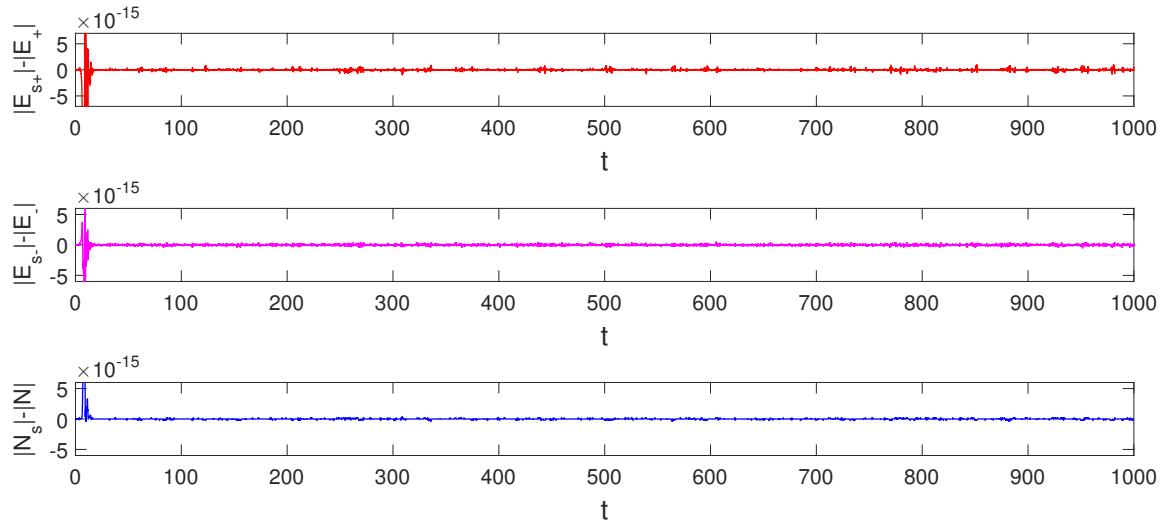


Figure 3: Synchronization errors of the electric fields and the density populations of the coupled systems of VCSELs given by Eqs. (1)-(3) and Eqs. (4)-(6)

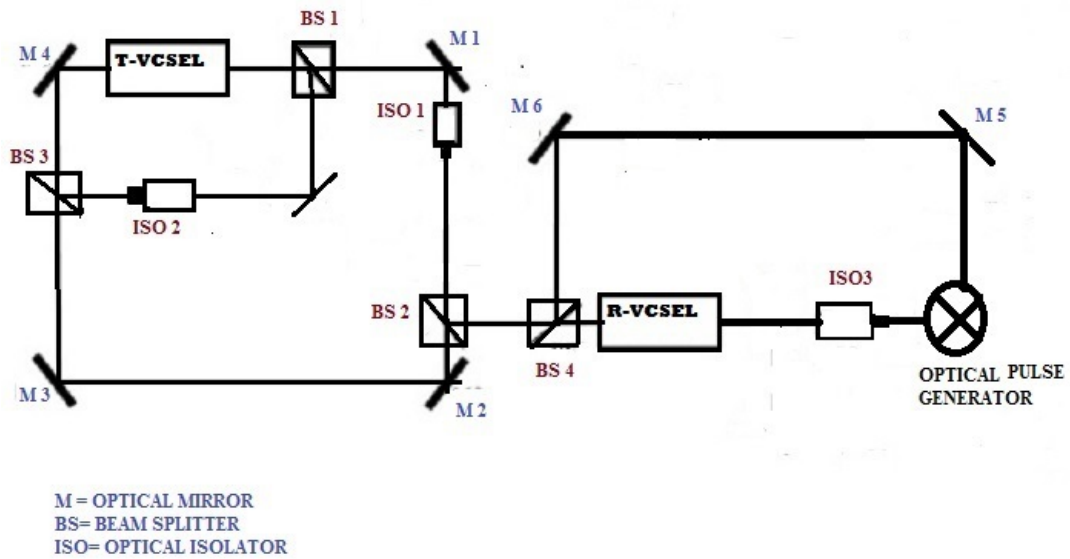


Figure 4: A schematic diagram for the coupling of VCSELs used for data transmission

5.2. Algorithm for encryption and decryption

We present an algorithm for the encryption and decryption of an RGB image using the chaotic data sequence as above. We begin with the shuffling of data using the chaotic time series. We also shuffle the pixel values of the image so that it becomes totally muddled. This pixel-level permutation can disrupt the correlation of the adjoining pixels. Furthermore, we employ a bit-level permutation, to change the bits of each pixel value of the shuffled sequence by a constant matrix. The processes are stated successively as follows.

Shuffling of data using chaotic time series.

- $A \leftarrow$ read (Image), where A is matrix (whose elements are called the voxel values or pixel values) of order $m \times l \times k$. Usually, in an RGB color image, $k = 3$ and so A is a three-dimensional matrix.
- Convert $A_{m \times l \times k}$ into one array, e.g., $T_{m,l,k} = [a_{1,1,1}, a_{1,2,1}, \dots, a_{m,l,k}]$.
- Having obtained the chaotic sequence $E_{vec}^- = E_1^-, E_2^-, E_3^-, \dots, E_j^-$, we choose $m \times l \times k$ data of E_- , after discarding first $j_0 (< j)$ number of values as those may not exhibit chaos, by the formula

$$E_{m \times l \times k}'^- = \text{uint8}(\text{round}(\text{abs}(E_i^-) \times 10^{10}))$$

, where $i = j_0, j_0 + 1, \dots, j_0 + m \times l \times k$, and arrange $E_{m \times l \times k}'^-$ in ascending order.

- *Pixel-level permutation.* Operate the BitXor function on each $T_{i,j,k}$ and $E_i'^-$, so that the pixels get shuffled. Thus, the pixel positions are changed and one obtains the following shuffled sequence

$$Q_{m,l,k} = [Q_{1,1,1}, Q_{1,2,1}, Q_{1,3,1}, \dots, Q_{m,l,k}].$$

Bit-level permutation.

Here, we change the bits of each pixel value of the shuffled sequence using a constant matrix that is to be formed using the initial conditions and the parameter values which exhibit chaos.

- Form the matrix M as: Let $d_1 = \max(m, l, k)$ and $d_2 = \min(m, l, k)$. Define $s_i = (x_i + m \times l \times k) / (2^{16} + m \times l \times k)$ for $i = 1, 2, \dots, r$ with the initial condition x_i and $m_i = \text{uint8}(\text{mod}(s_i \times 10^{16}, 1))$. Here, the factor 2^{16} is considered to make s_i much smaller than the unity, and that no recurrence occurs in the decimal representation of s_i . Also, in the definition of m_i , s_i is multiplied by 10^{16} in order to retain the values of m_i up to 16 significant digits (for security reason). Then

$$M = \begin{bmatrix} m_1 & m_2 & m_2 & \dots & m_r \\ \dots & \dots & \dots & \dots & \dots \\ m_r & m_1 & m_2 & \dots & m_{r-1} \end{bmatrix}. \quad (7)$$

- Divide each sequence of $Q_{m,l,k}$ into a matrix of order $r \times r \times (m \times l \times k) / r$, where r is one of the divisors of $m \times l \times k$.

- Do bit-level operation between each matrix of order $r \times r$ and the matrix M .
- Repeat the previous step until $\frac{m \times l \times k}{r}$ number of matrices have executed a round of bit-level permutation operation. Finally, we get the bit-level permutation matrix $P_{m \times l \times k}$ of the original image.

Encryption process.

We use the key vector $K_{y(m \times l \times k)}$ as in Sec. 5.1 to encrypt the permutation vector $P_{m \times l \times k}$ using the formulas, given by, $D_1 = \text{mod}((P_1 \oplus D_0), 256) \oplus \text{mod}((Q_1 \oplus K_{y1}), 256)$, $D_i = \text{mod}((P_i \oplus D_{i-1}), 256) \oplus \text{mod}((Q_i \oplus K_{yi}), 256)$, where D_0 is a constant vector of order $m \times l \times k$, $i = 2, \dots, m \times l \times k$. We then repeat the previous process(es) until the full encryption is done, and we get the cipher image as $CI \leftarrow \text{reshape}(D, m, l, k)$

Thus, following the above processes one can encrypt an image using the chaos vectors E_{\pm} , N and n . In Fig. 5 we show how a VCSEL is used for encryption and decryption of images or data through synchronization of master and slave lasers. Next, we now demonstrate the decryption algorithm as follows:

Decryption process.

The decryption process is the reverse process of encryption. Firstly, as soon as the synchronization of the two coupled VCSELs is achieved, the receiver obtains the cipher image, as well as, the initial conditions and the parameter values (those in the process of encryption) to generate the key. Here, the the key for decryption can be generated from the slave laser by the same way as in the process of encryption. Secondly, having obtained the cypher image and the key vectors we should repeat the same process as in the processes of shuffling the data and bit-level permutation.

Finally, we should use the BitXOR operation between the cypher image and the generated key vectors to recover the image data vectors, i.e., the decrypted cipher image (DCI) using the formulas as

$$D'_1 = \text{mod}((P'_1 \oplus D'_0), 256) \oplus \text{mod}((Q'_1 \oplus K_{y1}), 256),$$

$$D'_i = \text{mod}((P'_i \oplus D'_{i-1}), 256) \oplus \text{mod}((Q'_i \oplus K_{yi}), 256),$$

where $i = 2, \dots, m \times l \times k$; D'_i stands for the inversion of D_i , P'_i is the bit-level permutation vector which is generated from CI and Q'_i is the pixel shuffling vector of CI . We repeat the process(es) until the decryption of the cipher image is completed, and we recover the original image. After the original image A is recovered, reshape it as $A \leftarrow \text{reshape}(D'_{m,l,k})$.

6. Security analysis of encrypted image

In this section we will test and analyze our proposed cryptosystem whether it is resistant to statistical and differential attacks. In fact, the cipher image (CI) remains secured under the process of data transmission because the secrete key, which is based on the initial conditions and the range of parameters, securely passes through the communication channel during the synchronization of the couple system of VCSELs. The security analysis is given in subsections 6.1-6.6 which include the analysis of key space, differential attack resistance, histogram,

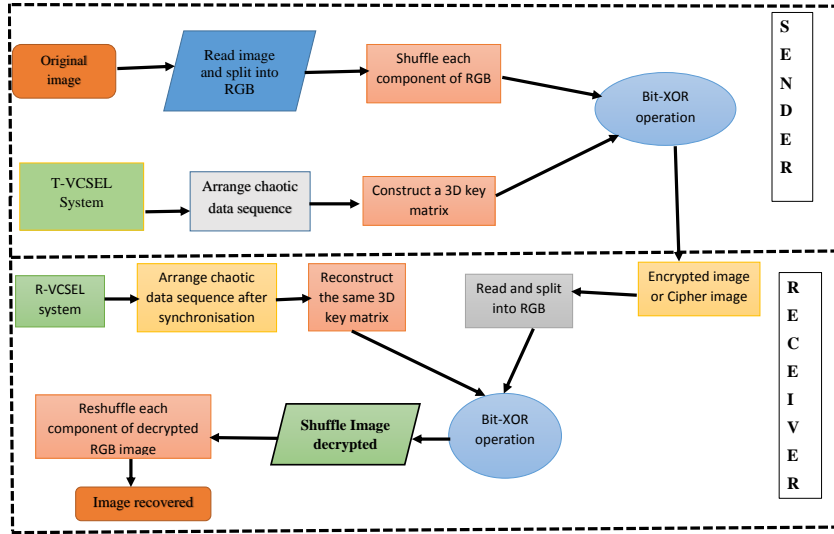


Figure 5: A pictorial diagram showing the encryption and decryption of images through chaotic medium.

correlation coefficient, quantile-quantile plot and the entropy analysis. To this end, we consider a 400×300 image “Autumn Leaves” as in Fig. 6(a). It is shown that even a small change of the key development can’t help recover images though the synchronization, i.e., the encryption is free from any brute force attack.

6.1. Key space and sensitivity analysis

The numerical set of values of E_{\pm} and N , which exhibit chaos under suitable initial conditions and parameters (as in Sec. 2) are arranged to establish the key vectors. We carry out the analysis of the key space attack resistance and the sensitivity analysis to get more secured data against any brute force attack effectiveness. The key space mainly consists of a wide number of key vectors which are generated by the solutions of the dynamical system of Eqs. (1)-(3) for the master laser which exhibit chaos. Each key vector is so generated that its elements lie between $0 - 225$ or in between $0 - 511$ as per the size of the image (e.g., $256 \times 256 \times 3$, 400×300 , $512 \times 512 \times 3$ etc.). These key vectors are then used for encoding the RGB image by the proposed algorithm as in Sec. 5. Here, any wrong key representation for decrypting the image gives an incorrect set of pixel values which is again a blur image. For key space analysis, we consider the initial condition that is used to generate chaos in the VCSELs and the key matrix to be of the order four for which we have $(10^{16})^4$ possible key elements. Again in Sec. 5.1 for the generation of key, we have $(10^{10} \times 10^{10}) = 10^{20}$ number of possible data set which represents the key elements. Also, in the process of encryption and key representation using the BitXor operation (8 bit operation), each layer of matrices has order 4. So, if N_0 denotes the total number of iterations in the encryption and decryption processes, then the total no of possible key

is $N_0 \times 2^8 \times 10^{64} \times 10^{20} \approx N_0 \times 2^{288}$, which is large enough to determine the key i.e. it is free from brute force attack.

The dynamical systems of VCSELs are sensitive to initial conditions, a small change of which can result into a different kind of solution, and hence an incorrect image or blur image even if the synchronization is achieved. The initial conditions by which the system exhibits chaos are mainly used for encoding and decoding the dataset. However, if a small change of values of E_{\pm} occur, e.g., from $E_{\pm} = 0.001$ to $E_{\pm} = 0.0015$, a different kind of key will be generated by which the particular image or information may not be recovered.

The steps for the generation of key as in Sec. 5.1 should also be followed in order. Otherwise, any change in between the steps results into an incorrect key, i.e., an incorrect representation of the image. In this case, the position of each pixel values of the image matrix will be changed and the effectiveness of displaying the image will result into a blur image. Thus, it may not be easy to recover the image even if one guesses a value of the key, i.e., the image will be transmitted to the receiver section secretly. In the receiver section, the key vectors are generated for decryption of the image through the synchronization of coupled VCSELs. Here, one must note that the generation of the key matrix must be only once throughout the synchronization. Fig. 6 shows the decryption of the image “Autumn Leaves” with correct and incorrect keys by the process as described above.

6.2. Differential attack resistance

To be resistant to a differential attack, a good cryptosystem must ensure that any small change or modification in the plain image results into a significant difference in the cipher image. In the formation of cipher image, since the pixel values of the plane image are taken in a proper order it is very difficult for

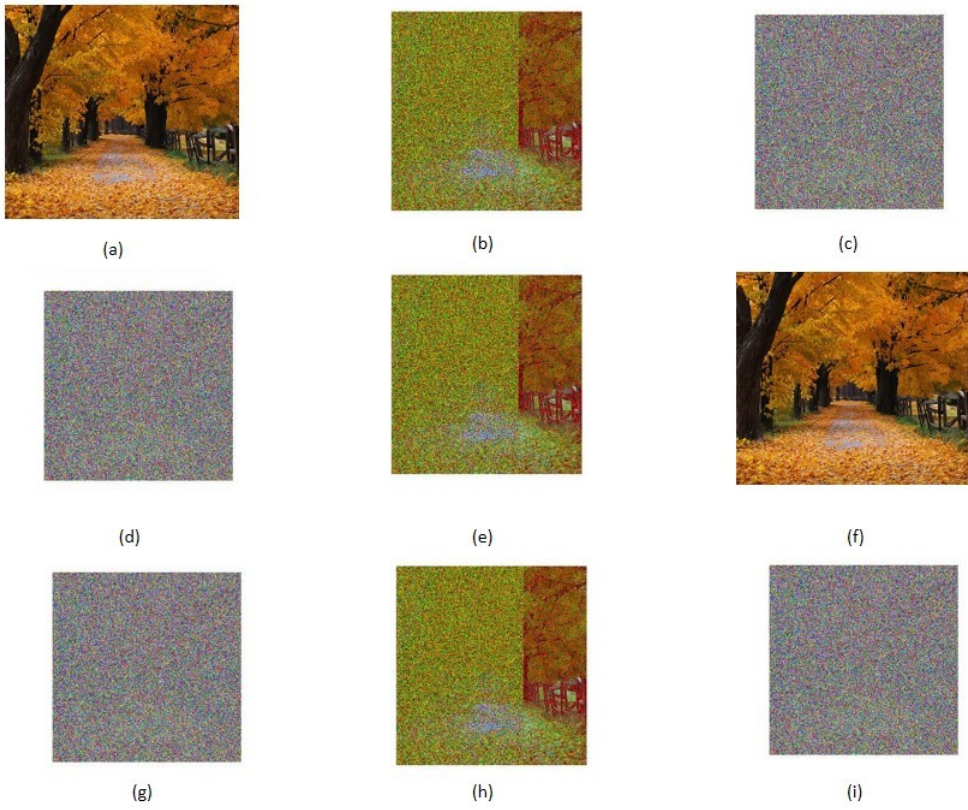


Figure 6: Encryption and decryption using the correct and wrong keys. Subfigures (a)-(c) indicate the encryption process. While subfigures (d)-(f) show the decryption process using the right key, subfigures (g)-(i) correspond to the incorrect image or blur image using a wrong key.

| | R | G | B |
|------|-------|-------|-------|
| NPCR | 99.73 | 99.78 | 99.74 |
| UACI | 33.23 | 33.27 | 33.14 |

Table 1: The measures of the number of pixels change rate (NPCR) and the unified average changing intensity (UACI) for an RGB image are shown.

hackers to recover the image even if they can make a small change of the pixel values for which a different cipher image is created thereby resisting the differential attack efficiently. To test the effects of only one change of pixel value from the plain image to the cipher image, we introduce two common measures, one the number of pixels change rate (NPCR) and other the unified average changing intensity (UACI). They are defined as follows:

$$NPCR = \frac{\sum_{i,j}^{m,n} D(i, j)}{m \times n} \times 100, \quad (8)$$

where $D(i, j)$ represents the change of the pixel values from the plain image to the cipher image due to the encryption process, i.e.,

$$D(i, j) = \begin{cases} 0 & \text{when } P(i, j) = CI(i, j) \\ 1 & \text{when } P(i, j) \neq CI(i, j). \end{cases} \quad (9)$$

As an illustration, we show an example of how the pixel values are changed from the plane image to the cypher image in the process of encryption.

$$\begin{aligned} P(1, 15, 1) &= 210, & CI(1, 15, 1) &= 17 \\ P(4, 4, 1) &= 185, & CI(4, 4, 1) &= 3 \\ P(200, 5, 2) &= 25, & CI(200, 5, 2) &= 2 \\ P(100, 100, 2) &= 81, & CI(100, 100, 2) &= 243 \\ P(10, 18, 3) &= 31, & CI(10, 18, 3) &= 224 \\ P(25, 100, 3) &= 37, & CI(25, 100, 3) &= 238, \end{aligned} \quad (10)$$

where the matrix P (CI) corresponds to the plain (cypher) image and their values are in the range 0–255, i.e., integer modulo 256. As the pixel values are changed, we use UACI to determine the average intensity of the difference between the original and the encrypted image, where

$$UACI = \frac{1}{m \times n} \sum_{i,j}^{m,n} \frac{|P(i, j) - CI(i, j)|}{255} \times 100. \quad (11)$$

Next, we show the results of NPCR and UACI in Table 1. It is evident that the scheme has high NCPR values with satisfactory UCAI values giving a resistant to any differential attack.

6.3. Comparison of times for image encryption with some existing schemes

The proposed algorithm is tested using Matlab 2016a in a laptop with 2.20 GHz processor Intel Core i3 – 2328 CPU, 4GB RAM, and Windows 8, 64-bit operating system. To this end, we consider the RGB Lena.jpg image of different sizes ($256 \times 256 \times 3$, $512 \times 512 \times 3$ and $1024 \times 1024 \times 3$). The average encryption/decryption times (in seconds) using different

schemes proposed in different articles are compared with our algorithm as given in Tables 2 and 3. It is seen that our scheme provides less time to encrypt/decrypt an image than the existing ones.

| RGB (Image size) | Time (Our scheme) | Time (Ref. [3]) | Time (Ref. [9]) | Time (Ref. [14]) |
|-----------------------------|-------------------|-----------------|-----------------|------------------|
| $256 \times 256 \times 3$ | 1.01 | 1.05 | 1.56 | 2.85 |
| $512 \times 512 \times 3$ | 1.83 | 2.01 | 2.34 | 4.43 |
| $1024 \times 1024 \times 3$ | 4.6 | 5.06 | 5.56 | 7.81 |

Table 2: Different encryption times (in seconds) of an RGB (*Lena.jpg*) image using different schemes are shown to ensure that our proposed scheme provides relatively less time to encrypt and decrypt an image.

| RGB (Image size) | Time (Our scheme) | Time (Ref. [3]) | Time (Ref. [9]) | Time (Ref. [14]) |
|-----------------------------|-------------------|-----------------|-----------------|------------------|
| $256 \times 256 \times 3$ | 1.0625 | 1.0841 | 2.36 | 3.25 |
| $512 \times 512 \times 3$ | 4.17 | 4.393 | 6.24 | 8.43 |
| $1024 \times 1024 \times 3$ | 17.13 | 17.356 | 35.246 | 48.321 |

Table 3: Different encryption times (in seconds) of an RGB (*Autumn leaves.jpg*) image using different schemes are shown to ensure that our proposed scheme provides relatively less time to encrypt and decrypt an image.

6.4. Histogram analysis

A histogram analysis corresponding to an image is mainly concerned with the distribution of the pixel (intensity) values within the image. Any encryption scheme is said to be secured if the encrypted image can have a uniform histogram to resist any statistical attacks. The histograms of the original RGB image “Autumn Leaves” and the corresponding cipher image are shown in Fig. 7.

We note that for an RGB image, the ordered pixels are scrambled or manipulated and their distribution is studied with the help of a chart representing the distribution of the pixels in the range 0 – 255. The q -th gray level l_q of a gray image is represented by a function $\text{hist}(l_q) = n_q$, where n_q denotes the number of pixels in the image. In the diffusion phase, the positions of the image elements are then shuffled so that the statistical information of the original image remains unaltered. However, an additional layer of security will disguise the desired information, as reflected in the histogram (Fig. 7). It is also clear from Fig. 7 that the gray-scale values of the encrypted image (see the right panels d to f) are uniformly distributed over the interval [0 255], which is significantly different from that of the original image (see the left panels a to c). Thus, an attacker will be unable to infer any statistical information required to decode from the scheme. From the results of the pixel intensity distributions, it can be ascertained that the scheme also possesses good confusion properties.

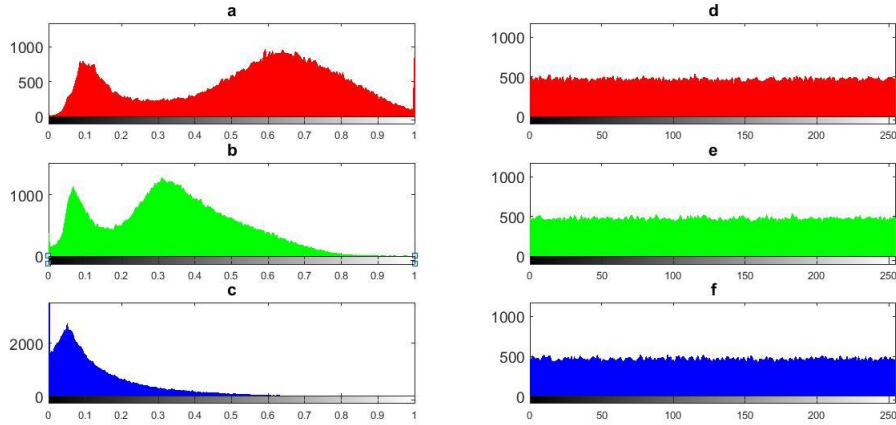


Figure 7: Histogram analysis: Subfigures (a), (b) and (c), respectively, correspond to the R, G and B components of the original image, and (d), (e) and (f) are those for the cipher image.

6.5. Correlation analysis

The adjacent pixels of the original image are highly correlated while distributed along the horizontal (H), vertical (V) and diagonal (D) directions. However, an ideal encryption algorithm ensures that for the encrypted image the correlation coefficients of the adjacent pixels is nearly zero to resist any statistical attack. The correlations of the adjacent pixels in the plain and cipher images are analyzed and compared as shown in Fig. 8.

To define the correlation coefficients, we first define the covariance between a pair of pixel values x and y as $Cov(x, y) = E[(x - E(x))(y - E(y))]$. Then the corresponding correlation coefficient is given by

$$\rho_{(x,y)} = \frac{Cov(x,y)}{\sigma(x)\sigma(y)}, \quad \sigma(x), \sigma(y) \neq 0, \quad (12)$$

where $E(x)$ and $E(y)$ are the means, and $\sigma(x)$ and $\sigma(y)$ are the standard deviations of the distribution of the pixel values which range from 0 to 255. The adjacent pixel values are placed horizontally, diagonally and vertically. The values of ρ are computed for the RGB image “Autumn Leaves” and the cipher image as given in Tables 4 and 5. From the computed values it

| ρ | R | G | B |
|--------|--------|--------|--------|
| H | 0.9041 | 0.8109 | 0.7347 |
| V | 0.8875 | 0.7748 | 0.6725 |
| D | 0.8551 | 0.7194 | 0.6094 |

Table 4: Correlation coefficients of a pair of adjacent pixel values of the plain image “Autumn Leaves” while distributed along the horizontal (H), vertical (V) and diagonal (D) directions.

is observed that the correlation coefficients for the cipher image are very low i.e., close to zero. This is also evident from the scatter diagrams for the RGB and the cipher images as in Fig. 8. We find that it is hard to correlate between the plain and the cipher images. For an encryption scheme to be efficient, it is

| ρ | R | G | B |
|--------|---------|---------|---------|
| H | -0.0008 | -0.0013 | 0.0056 |
| V | 0.0006 | 0.0017 | -0.0032 |
| D | 0.0036 | 0.0007 | -0.0013 |

Table 5: Correlation coefficients of a pair of adjacent pixel values, corresponding to the cipher image of “Autumn Leaves”, while distributed along the horizontal (H), vertical (V) and diagonal (D) directions.

imperative that the correlation coefficient between the adjacent pixels be minimal for the cipher image. This is what we have also obtained in the present analysis.

6.6. Q-Q plot and comparison

For a quantitative analysis of the red, green and blue components of the encrypted RGB image “Autumn Leaves” as in Fig. 6(a), we plot the quantiles of input sample (QIP) against the standard normal quantile (SNQ), i.e., the quantile-quantile (Q-Q) plot, which is used to check whether the points of the sample data set fall approximately along a reference line (e.g., the 45-degree reference line). In general, the basic idea is to compute theoretically the expected value for each data point based on the distribution under consideration. If the data, indeed, follows the assumed distribution, then the points on the Q-Q plot will fall approximately on a straight line. From Fig. 9, it is evident that the data points of the red, green and blue fall approximately along the reference line. This approximate linearity of the points suggests that the data are normally distributed.

We ought to mention that our present encryption algorithm significantly modifies that proposed by Li *et al.* [2]. The modification is mainly due to the use of the BitXor function in the bit-level permutation. The necessity for such a modification is based on some reasons, namely,

- Firstly, using the algorithm of Li *et al.* [2], the matrix multiplication between the 4×4 constant matrix and the

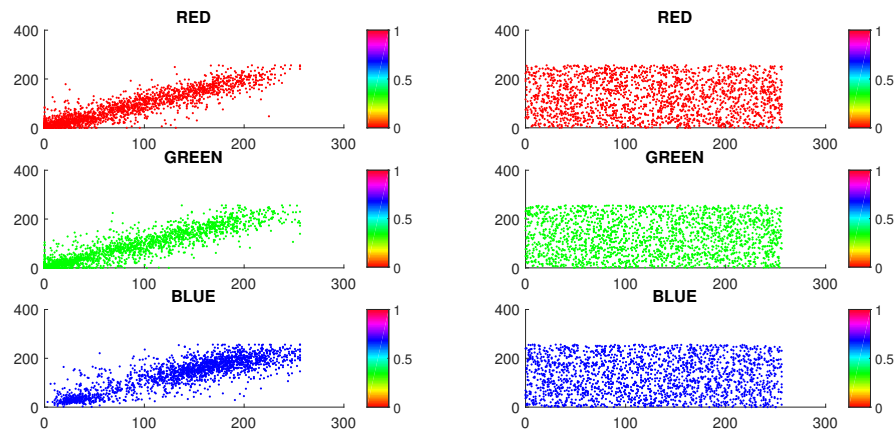


Figure 8: Scatter plots of the correlation coefficients of the adjacent pixels of the original RGB image (left panel) and the cipher image (right panel). The subplots a, b and c (d, e and f) are corresponding to the R, G, and B components of the original image (cipher image).

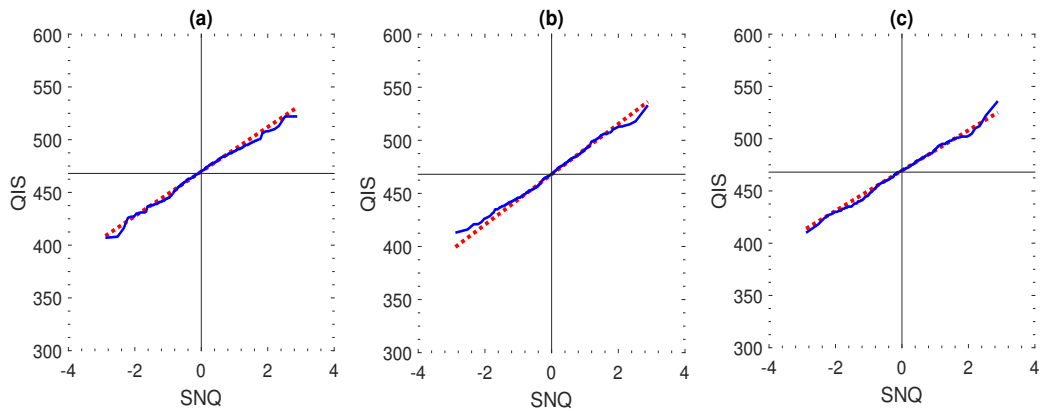


Figure 9: Q-Q plots of the (a) Red (b) Green and (c) Blue components of the encrypted RGB image using the algorithm as in Sec. 5. The acronyms SNQ and QIS, respectively, stand for the standard normal quantile (red dotted lines) and the quantile of input sample (blue dashed lines).

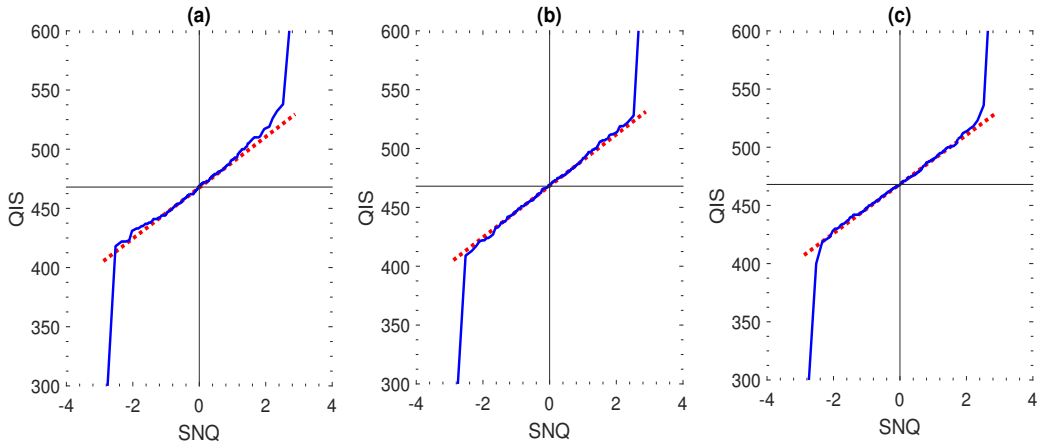


Figure 10: Q-Q plots of the (a) Red (b) Green and (c) Blue components of the encrypted RGB image using the algorithm as in Ref. [2]. The acronyms SNQ and QIS, respectively, stand for the standard normal quantile (red dotted lines) and the quantile of input sample (blue dashed lines).

pixel-shuffled matrix of order $4 \times 4 \times \frac{MN}{4}$ in the bit-level permutation takes much longer time than using our proposed algorithm. Furthermore, the encryption/decryption algorithm of Li *et al.* [2] may not be a good resistant to any time attack or any kind of brute force attack.

- Secondly, Li *et al.* [2] considered a two-dimensional digital image matrix, however, in the present theory, we have considered an RGB image which has more pixel values than the digital image matrix. So, in the diffusion process, a simple scalar addition of the bit-level permutation matrix with the chaotic data set makes the decryption process much more complicated, however, the bit-wise XOR operation, as in the present algorithm, causes no such problem in addition. Thus, the encryption scheme in Ref. [2] may be safe, but may not be much secured compared to our present algorithm.

In order to compare our proposed algorithm with that in Ref. [2], and to show why our algorithm provides better security for encryption and decryption, we consider the RGB image “Autumn Leaves” as in Fig. 6(a). The results for the Q-Q plots are displayed in Fig. 10. Comparing the results in Figs. 9 with 10, one can conclude that the encryption algorithm in Ref. [2] has some limitations as evident from the singularities at some points of the data set, which are, however, removed by the modified algorithm as proposed in the present work.

6.7. Entropy Analysis

Here, we present another statistical measure of uncertainty for the RGB image. As per the Shannon entropy [18], it is the expected value of the information contained in an image, and is defined by

$$H(X) = E[I(X)] = -E[\ln(P(X))], \quad (13)$$

where E is the expected value operator and I is the information content of the random variable X . Equation (13) can also be written as

$$H(x) = \sum_{i=0}^{255} P(x_i) I(x_i) = - \sum_{i=0}^{255} P(x_i) \log_2 P(x_i). \quad (14)$$

We assume that there are 256 values of the information source in Red, Green and Blue colors of the image with the same probability. We can get the perfect entropy $H(X) = 8$, corresponding to a truly random sample [19]. The information entropy of Red, Green and Blue colors of the plain and their corresponding encrypted images are computed and displayed in Tables 6 and 7. To this end, we choose three different images for the three different samples as in Fig. 11 (one of which is the “Autumn Leaves” image). From Table 7, it is evident that the entropy values corresponding to the encrypted RGB image are close to 8 as expected for a true random sample.

| Image index | R | G | B |
|-------------|--------|--------|--------|
| Fig. 11(a) | 7.7644 | 7.4035 | 6.0690 |
| Fig. 11(b) | 7.9450 | 7.9556 | 7.0454 |
| Fig. 11(c) | 5.6564 | 6.8519 | 6.6589 |

Table 6: Entropy values corresponding to the original images as in Figs. 11(a)-11(c).

7. Conclusion

We have investigated the chaos and synchronization properties of electric field polarizations and the carrier population densities in a free-running vertical-cavity surface-emitting laser (VCSEL). A two-way coupling of master and slave lasers in



Figure 11: Three different images for which the entropy values are calculated. The corresponding entropy values are given in Tables 6 and 7.

| Image index | R | G | B |
|-------------|--------|--------|--------|
| Fig. 11(a) | 7.9908 | 7.9906 | 7.9907 |
| Fig. 11(b) | 7.9903 | 7.9908 | 7.9902 |
| Fig. 11(c) | 7.9878 | 7.9874 | 7.9891 |

Table 7: Entropy values corresponding to the cipher images of Figs. 11(a)-11(c).

VCSELs is considered, which is shown to exhibit hyperchaos and synchronization with a high level of similarity. The coupled VCSELs are then used as a sender and a receiver for the communication of image or data. We have also proposed a modified chaos-based image encryption algorithm using the pixel- and bit-level permutations which is robust, faster and simpler in encryption/decryption compared to many other chaos-based cryptosystems [3, 9, 14]. The new cryptosystem is analyzed and compared with a recently proposed one [2]. It is shown (by the security analysis) that the proposed cryptosystem is resistant to various types of attacks and is efficient for secure communications in nonlinear optical media.

Acknowledgements

This work was supported by UGC-SAP (DRS, Phase III) with Sanction order No. F.510/3/DRS-III/2015(SAPI), and UGC-MRP with F. No. 43-539/2014 (SR) and FD Diary No. 3668.

References

- [1] L. Xu, X. Gou, Z. Li, J. Li, A novel chaotic image encryption algorithm using block scrambling and dynamic index based diffusion, *Opt. Las. Eng.* 91 (2017) 41-52.
- [2] Y. Li, C. Wang, H. Chen, A hyper-chaos-based image encryption algorithm using pixel-level permutation and bit-level permutation, *Opt. Las. Eng.* 90 (2017) 238-246.
- [3] S.E. Assad, M. Farajallah, A new chaos-based image encryption system, *Signal Process.: Image Commun.* 41 (2016) 144-157.
- [4] D. Xiao, Q. Fu, T. Xiang, Chaotic Image Encryption of Regions of Interest, *Int. J. Bifur. and Chaos*, 26 (2016) 1650193.
- [5] Y. Xu, H. Wang, Y. Li, B. Pei, Image encryption based on synchronization of fractional chaotic systems, *Commun. Nonlinear Sci. Numer. Simulat.* 19 (2014) 3735-3744.
- [6] M. Virte, K. Panajotov, M. Sciamanna, Bifurcation to nonlinear polarization dynamics and chaos in vertical-cavity surface-emitting lasers, *Phys. Rev. A* 87 (2013) 013834.
- [7] S. Banerjee, L. Rondoni, S. Mukhopadhyay, A. P. Misra, Synchronization of spatiotemporal semiconductor lasers and its application in color image encryption, *Opt. Commun.* 284 (2011) 2278-2291.
- [8] T. M. Hoang, S. K. Palit, S. Mukherjee, S. Banerjee, Synchronization and secure communication in time delayed semiconductor laser systems, *Optik* 127 (2016) 10930-10947.
- [9] D. Socek, S. Li, S. Magliveras, B. Furht, Enhanced 1-D chaotic key based algorithm for image encryption, *IEE/CreateNet Secure Comm.*, pp. 406-408 (2005).
- [10] A. Daneshgar, B. Khadem, A self-synchronized chaotic image encryption scheme, *Signal Process.: Image Commun.* 36 (2015) 106-114.
- [11] K. Nosrati, C. Volos, A. Azemi, Cubature Kalman filter-based chaotic synchronization and image encryption, *Signal Processing: Image Communication* (2017), <https://doi.org/10.1016/j.image.2017.06.005>.
- [12] K. Iga, Vertical-Cavity Surface-Emitting Laser (VCSEL), *Proceedings of the IEEE*, 101 (2013) 2229-2233.
- [13] K. Panajotov, F. Prati, in *VCSELs*, edited by R. Michalzik (Springer-Verlag, Berlin, 2012), pp. 181-231.
- [14] B. Subramanyan, V. M. Chhabnia, T. G. S. Babu, Image encryption based on AES key expansion, *Second international conference on emerging applications of information technology*, 978-0-7695-4329-1//11 @ 2011 IEEE, pp. 217-220.
- [15] J. P. Hermier, M. I. Kolobov, I. Maurin, E. Giacobino *Quantum spin-flip model of vertical-cavity surface emitting laser*, *Physical Review A*, 65: 053825 [13 pages], 2002.
- [16] J. Martin-Regalado, F. Prati, M. San Miguel, N. Abraham, Polarization properties of vertical-cavity surface-emitting lasers, *IEEE J. Quantum Electron.* 33, (1997) 765.
- [17] R. Michalzik, K. J. Ebeling, *Operating Principles of VCSELs*, Springer Series in Photonics, 6 (2003) 53-98.
- [18] C. E. Shannon, *A Mathematical Theory of Communication*, *Bell System Technical Journal*, July 1948, p.623.
- [19] B. Stoyanov, K. Kordov, Image encryption using Chebyshev map and rotation equation, *Entropy* 17 (2015) 2117-2139.